Supplement of Atmos. Chem. Phys., 25, 4803–4831, 2025
https://doi.org/10.5194/acp-25-4803-2025-supplement

Atmospheric Chemistry and Physics
Open Access

Supplement of

Modelling of atmospheric variability in gas and aerosols during the ACROSS campaign 2022 of the greater Paris area: evaluation of the meteorology, dynamics and chemistry

Ludovico Di Antonio et al.

Correspondence to: Ludovico Di Antonio (ludovico.diantonio@lisa.ipsl.fr) and Matthias Beekmann (matthias.beekmann@lisa.ipsl.fr)

S1. Yields of semi-volatile organic compounds from oxidation of aromatic and terpene species

We present normalized SOA yields α_i in the 4 bins VBS approach with saturation concentrations from 1 to 10^3 µg m^{-3}; ΔH: enthalpy of products; the density of OA is assumed as 1.5 g cm^{-3}. Yields are from Zhang et al., (2013) and Murphy and Pandis, (2009), for the latter case for low NOx conditions. Yields are taken as equal independently of the initial oxidant (OH, NO_3 or ozone).

for low NOx conditions:

VOC precursors	**Mass yields of each bin**				**ΔH**
C* (µg m^{-3})	1	10	100	1000	**(kJ mol^{-1})**
ALK4	0.0	0.075	0.0	0.0	30
ALK5	0.0	0.300	0.0	0.0	30
OLE1	0.0045	0.009	0.060	0.225	30
OLE2	0.0225	0.435	0.129	0.375	30
ARO1	0.075	0.225	0.375	0.525	30
ARO2	0.075	0.300	0.375	0.525	30
TERP	0.1073	0.0918	0.3587	0.6075	30
HUMULENE	0.075	0.15	0.75	0.90	30
ISOP	0.009	0.03	0.015	0.0	30

for high NOx conditions:

VOC precursors	**Mass yields of each bin**				**ΔH**
C* (μg m^{-3})	1	10	100	1000	**(kJ mol^{-1})**
ALK4	0.0	0.0375	0.0	0.0	30
ALK5	0.0	0.15	0.0	0.0	30
OLE1	0.0008	0.0045	0.0375	0.15	30
OLE2	0.003	0.0225	0.0825	0.27	30
ARO1	0.03	0.165	0.30	0.435	30
ARO2	0.0015	0.195	0.30	0.435	30
TERP	0.012	0.1215	0.201	0.507	30
HUMULENE	0.075	0.15	0.075	0.90	30
ISOP	0.003	0.0225	0.015	0.0	30

The VOC species are in general lumped species used within the SAPRC-07 chemical gas phase mechanism (Carter, 2010). An exception is TERPEN for which α-pinene, β-pinene, limonene, and ocimene have same SVOC yields, but different rate constants:

ALK4 : essentially C5 and C6 Alkanes and some higher branched Alkanes,

ALK5 : C7-C22 n-Alkanes, C6-C16 Cycloalkanes, branched C8-C18 Alkanes

OLE1 : Propene, C4-C15 terminal Alkanes

OLE2 : Isobutene, C4-C15 Internal Alkenes, C6-C15 Cyclic or di-olefins, Styrenes

ARO1: Toluene, benzene, Ethyl benzene, C9-C13 Monosubstituted Benzenes

ARO2: Xylenes, Ethyl Toluenes, Dimethyl and Trimethyl Benzenes, Ethylbezenes, naphthalene, C8-C13 Di-, Tri-, Tetra-, Penta-, Hexa-substituted Benzenes, Unspeciated C10-C12 Aromatics

TERPEN: monoterpenes C10H16 as α-pinene, β-pinene, sabinene, δ^3-carene, limonene, ocimene and myrcene

HUMULENE : sesquiterpenes C15H24

ISOP : Isoprene C5H8

S2. Reaction list of the VBS scheme with functionalization and fragmentation, and non-volatile aerosol formation processes for POA, ASOA and BSOA

For the simulations presented in this work, a version of the VBS scheme allowing for functionalization, fragmentation and formation of non-volatile organic aerosol from semi-volatile organic compounds was activated. It to the scheme presented in (Cholakian et al., 2018), based on earlier work of (Shrivastava et al., 2013) and (Shrivastava et al., 2015). The chemical mechanism are described in Appendix H.6 for POA derived species and in H11 for ASOA and BSOA in the documentation of the CHIMERE model https://www.lmd.polytechnique.fr/chimere/docs/CHIMEREdoc_v2023.pdf. The description did not change with respect to the documentation of the 2020 version used for this work. All reactions are homogeneous gas phase reactions. Fragmentation processes correspond to the breakup of oxidized OA compounds in the atmosphere into smaller and thus more volatile molecules. For POA derived species, this process is only activated for compounds having undergone three oxidation reactions (O3POA).

Reaction	**Reactions kinetic rates (molec.cm^{-3}.s^{-1})**
Ageing Reactions for POA:	
Functionalization:	
for i=2 – 9: POA_i+OH→OH+1.075*$OPOA_{i-1}$	k=4.00e-11
for i=2 – 8: $OPOA_i$+OH→OH+1.075*$O2POA_{i-1}$	k=4.00e-11
for i=2 – 7: $O2POA_i$+OH→OH+1.075*$O3POA_{i-1}$	k=4.00e-11
Functionalization and fragmentation for oxidized compounds:	
for i=1 – 5: O3POAi+OH→OH+0.16125*$O3POA_1$+0.75*$O3POA_6$	k=4.00e-11
for i=6 –8:	
$O3POA_6$+OH→OH+0.16125*$O3POA_5$+0.75*$O3POA_7$	k=4.00e-11
$O3POA_7$+OH→OH+0.16125*$O3POA_6$+0.75*$O3POA_8$	k=4.00e-11
$O3POA_8$+OH→OH+0.16125*$O3POA_7$+0.75*$O3POA_8$	k=4.00e-11
Production of non-volatile organic aerosol	
for i=1 – 6: $OPOA_i$→ONVSOA	k=3e-4
for i=1 – 6: $O2POA_i$→O2NVSOA	k=3e-4

for i=1 – 6: $O3POA_i \rightarrow O3NVSOA$ k=3e-4

Ageing Reactions for ASOA and BSOA:

Functionalization and fragmentation

$ASOA_1$+OH->0.16125*$ASOA_1$+0.75*$ASOA_4$ k=1e-11

for i=2 – 4: $ASOA_i$+OH->0.16125*$ASOA_{i-1}$+0.75*$ASOA_4$ k=1e-11

$BSOA_1$+OH->0.16125*$BSOA_1$+0.75*$BSOA_4$ k=1e-11

for i=2 – 4: $BSOA_i$+OH->0.16125*$BSOA_{i-1}$+0.75*$BSOA_4$ k=1e-11

Production of non-volatile secondary aerosol from organic aerosols (the prefix “p-“ indicates that the species is in the particle phase.

for i=1 – 4: p-$ASOA_i$->p-ANVSOA k=3e-4

for i=1 – 4: p-$BSOA_i$->p-BNVSOA k=3e-4

Supplementary figures:

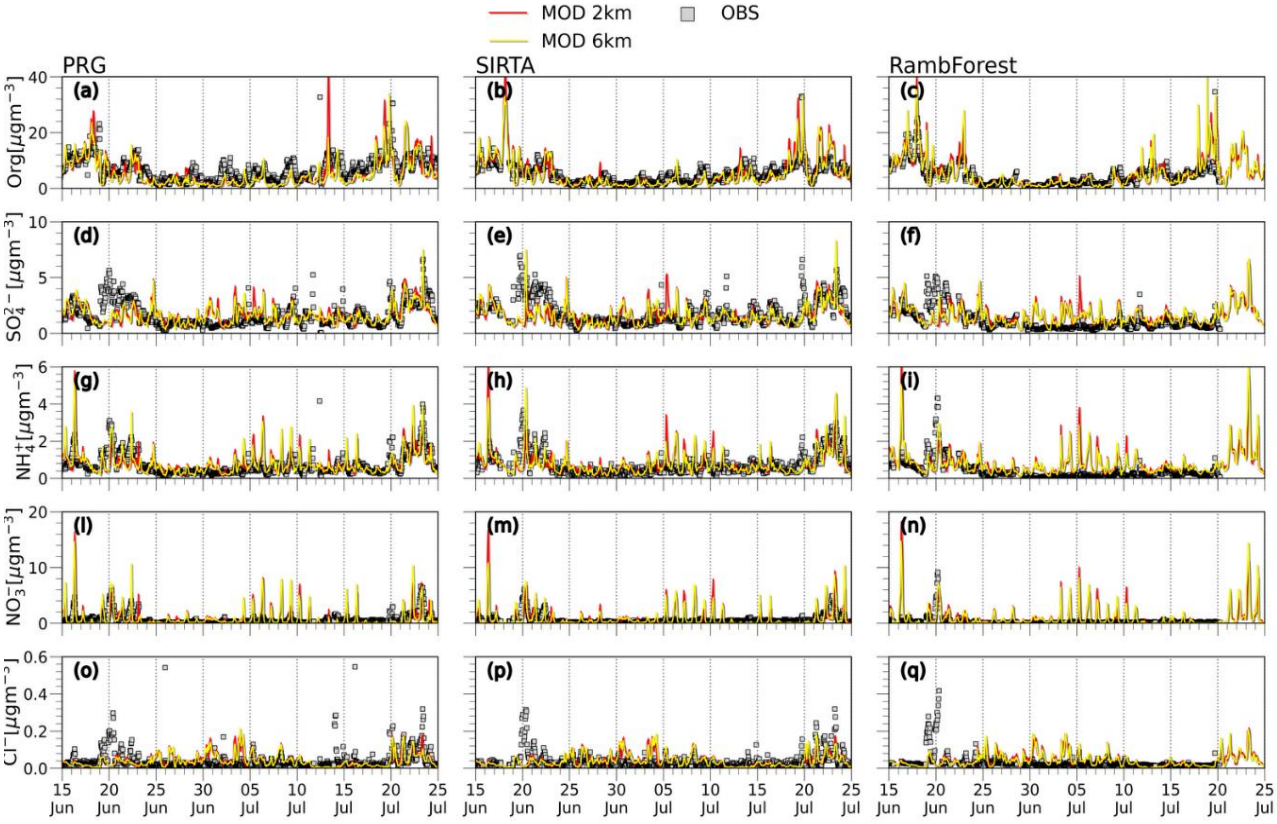

Figure S1: Observed and simulated PM_1 aerosol chemical composition at 2 (yellow) and 6 (red) km model resolution, at the three ACROSS campaign sites.

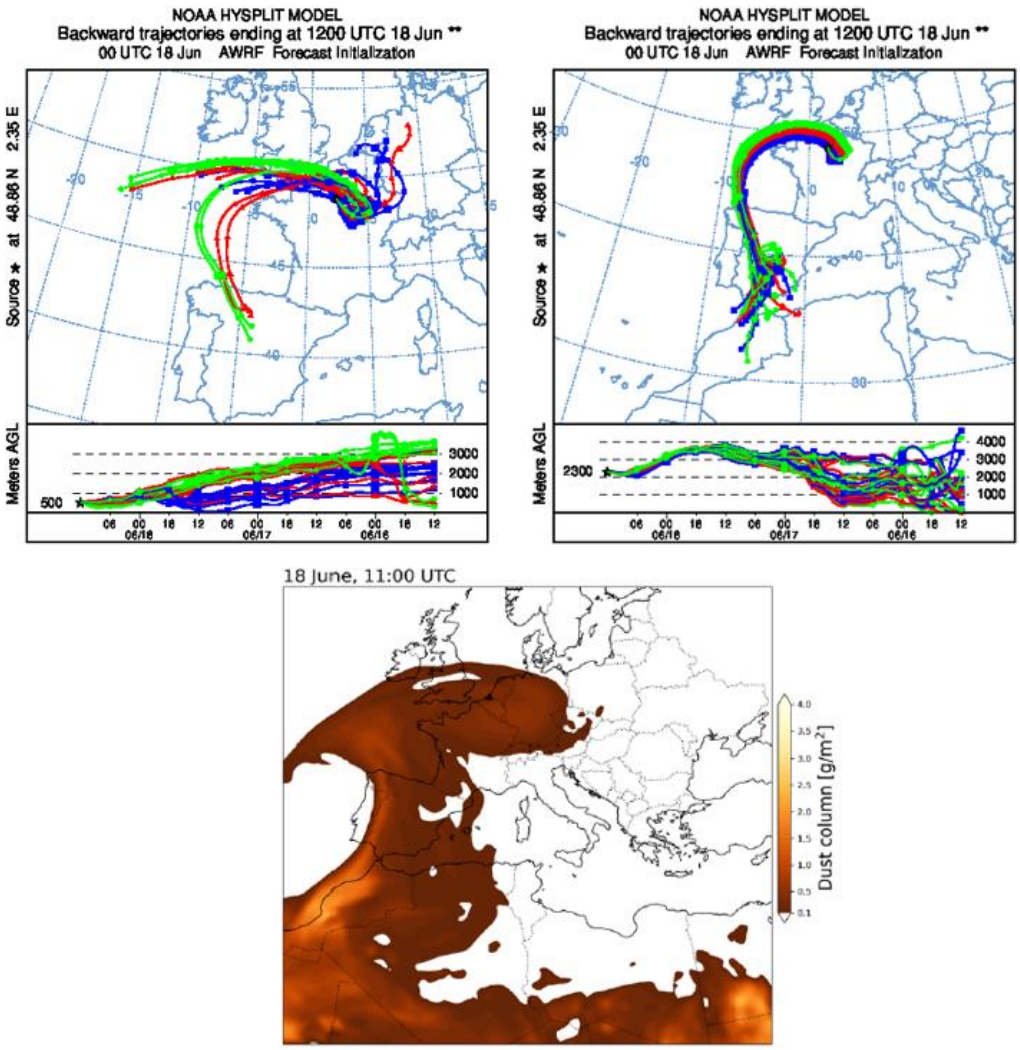

Figure S2 (Top) 3–day HYSPLIT backward trajectory simulations from (Siour and Di Antonio, 2023) for the 18 June 2022 starting in the center of Paris at an altitude of 500m (left) and 2000 m (right). (Bottom) Simulated dust columnar concentrations on the 18 June 2022 at 11:00 UTC. The dust plume reached northern Europe and the Paris area during the day.

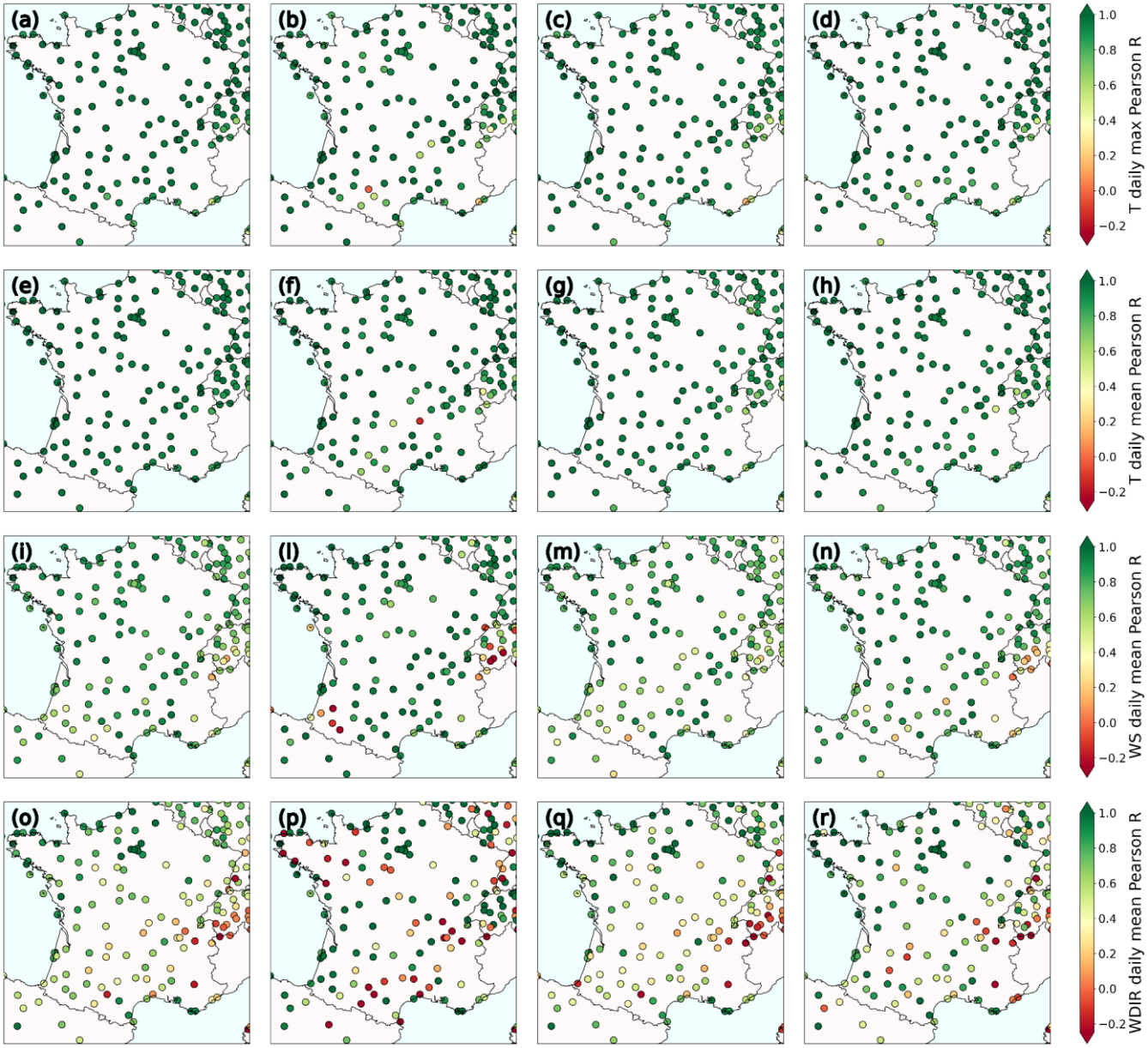

Figure S3: Daily Pearson correlation coefficient between WRF−CHIMERE model output and observations of the MIDAS database respectively for the full period (left column), the first heatwave (middle left column), the clean period (middle right column) and the second heatwave (right column); (a)–(d) for the temperature daily max, (e)–(h) temperature daily mean, (i)–(n) wind speed daily mean and (o)–(r) wind speed daily mean.

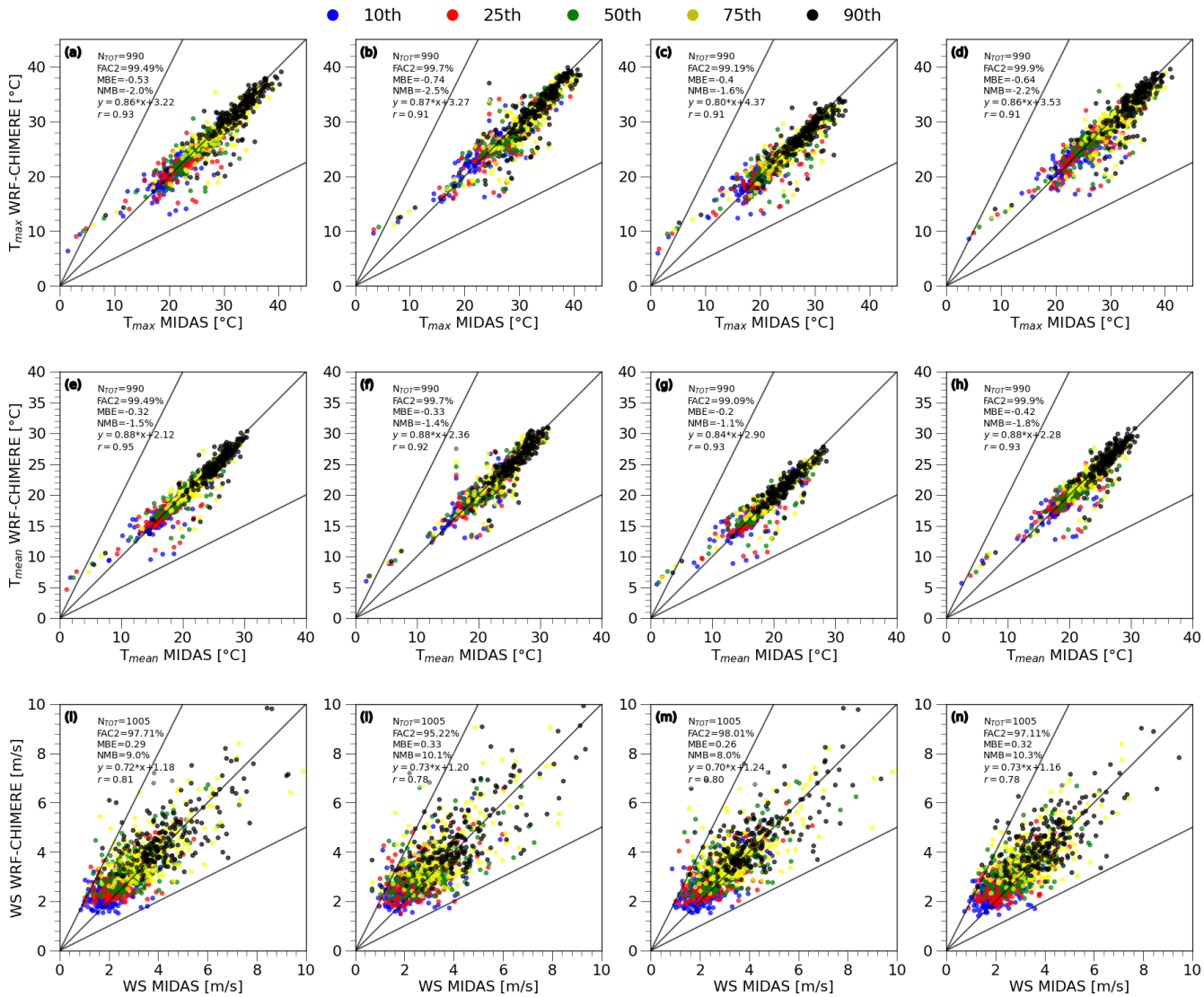

Figure S4: Percentile analysis of the WRF–CHIMERE simulated meteorological parameters compared to the MIDAS database observations, respectively for the full period (left column), the first heatwave (middle left column), the clean period (middle right column) and the second heatwave (right column) for the (a)–(d) temperature max, (e)–(h) temperature mean, (i)–(n) wind speed. Statistical metrics are calculated from data merged for all sites: NTOT number of observations, FAC2 fraction of points within a factor of 2 limit, MBE mean bias error, NMB normalized mean bias, linear fit equation, R correlation coefficient. The percentiles are calculated on the entire period of simulation and for each site available.

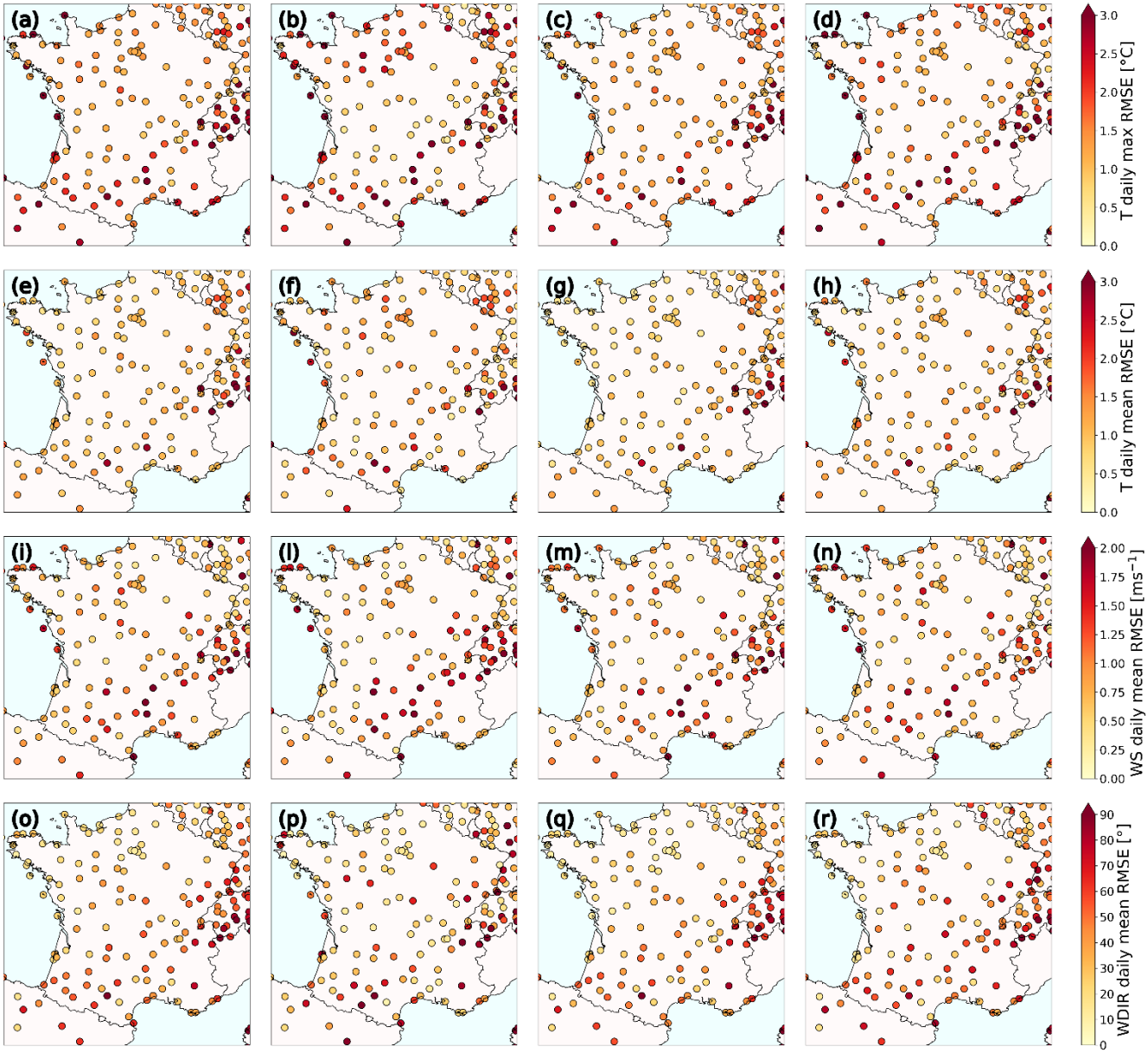

Figure S5: Daily root mean square error (RMSE) coefficient between WRF–CHIMERE model output and observations of the MIDAS database respectively for the full period (left column), the first heatwave (middle left column), the clean period (middle right column) and the second heatwave (right column); (a)–(d) for the temperature daily max, (e)–(h) temperature daily mean, (i)–(n) wind speed daily mean and (o)–(r) wind speed daily mean.

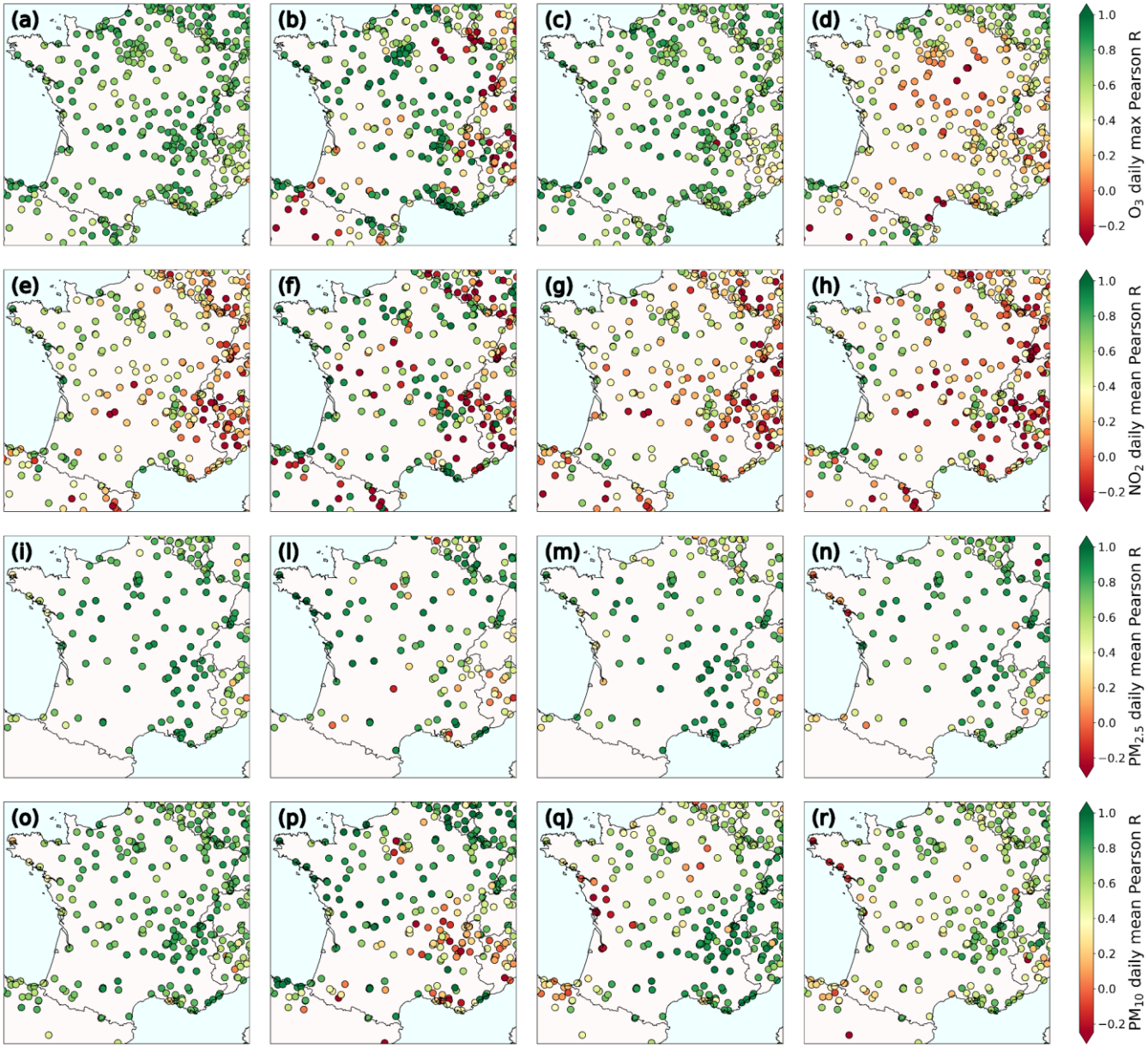

Figure S6: Daily Pearson correlation coefficients between WRF–CHIMERE output and EEA observations, respectively for the full period (left column), the first heatwave (middle left column), the clean period (middle right column) and the second heatwave (right column) for the (a)–(d) O3 daily max, (e)–(h) NO2 daily mean, (i)–(n) PM2.5 daily mean and (o)–(r) PM10 daily mean.

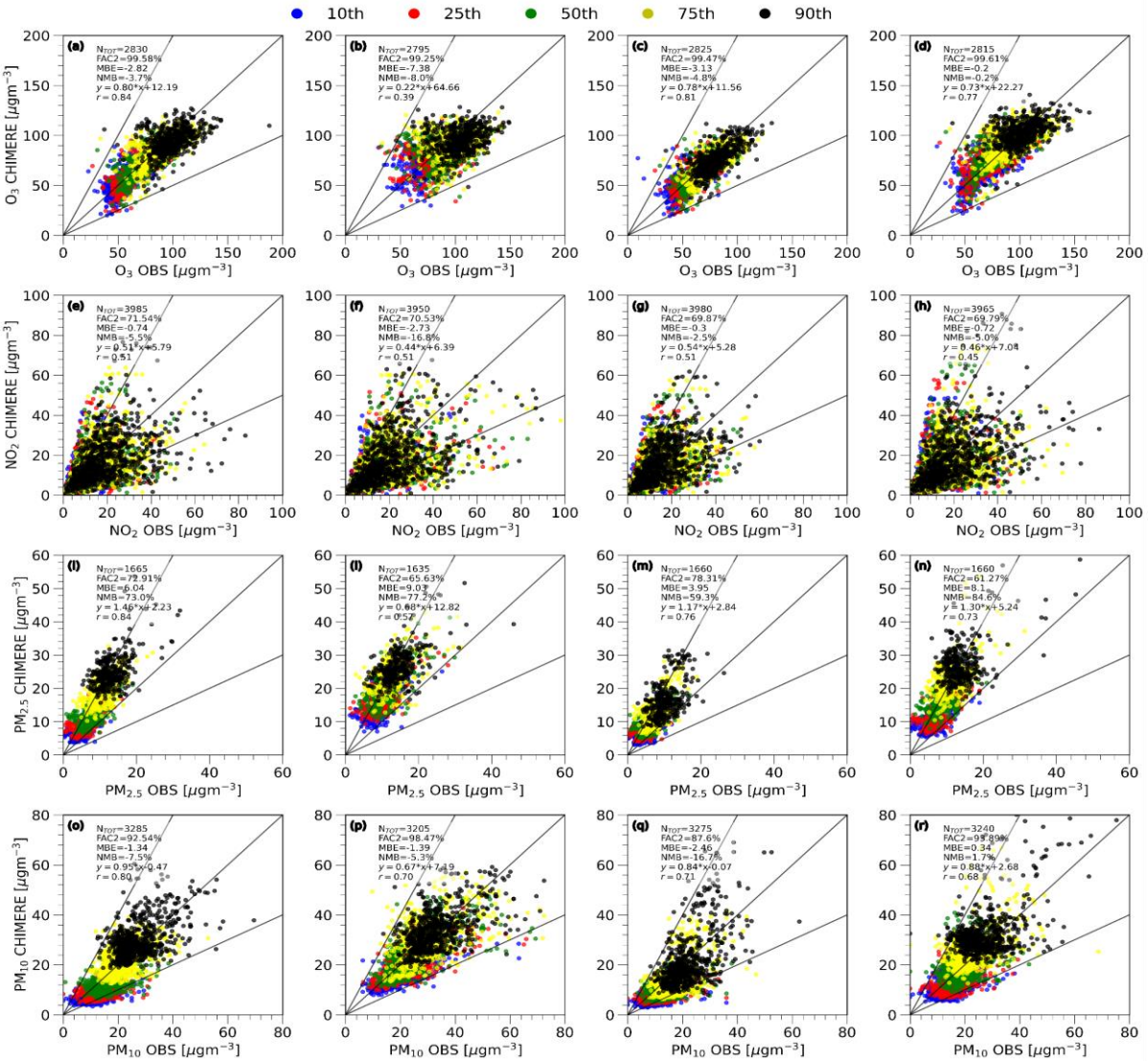

Figure S7: Percentile analysis of the WRF–CHIMERE simulated aerosol load and gaseous compounds compared to EEA observations, respectively for the full period (left column), the first heatwave (middle left column), the clean period (middle right column) and the second heatwave (right column) for the (a)–(d) O3, (e)–(h) NO2, (i)–(n) PM2.5, (o)–(r) PM10. Statistical metrics are calculated from data merged for all sites: NTOT number of observations, FAC2 fraction of points within a factor of 2 limit, MBE mean bias error, NMB normalized mean bias, linear fit equation, R correlation coefficient. Percentiles are calculated from the daily max values for O3, and from the daily means for PM10, NO2, PM2.5. The percentiles are calculated on the entire period of simulation and for each site available.

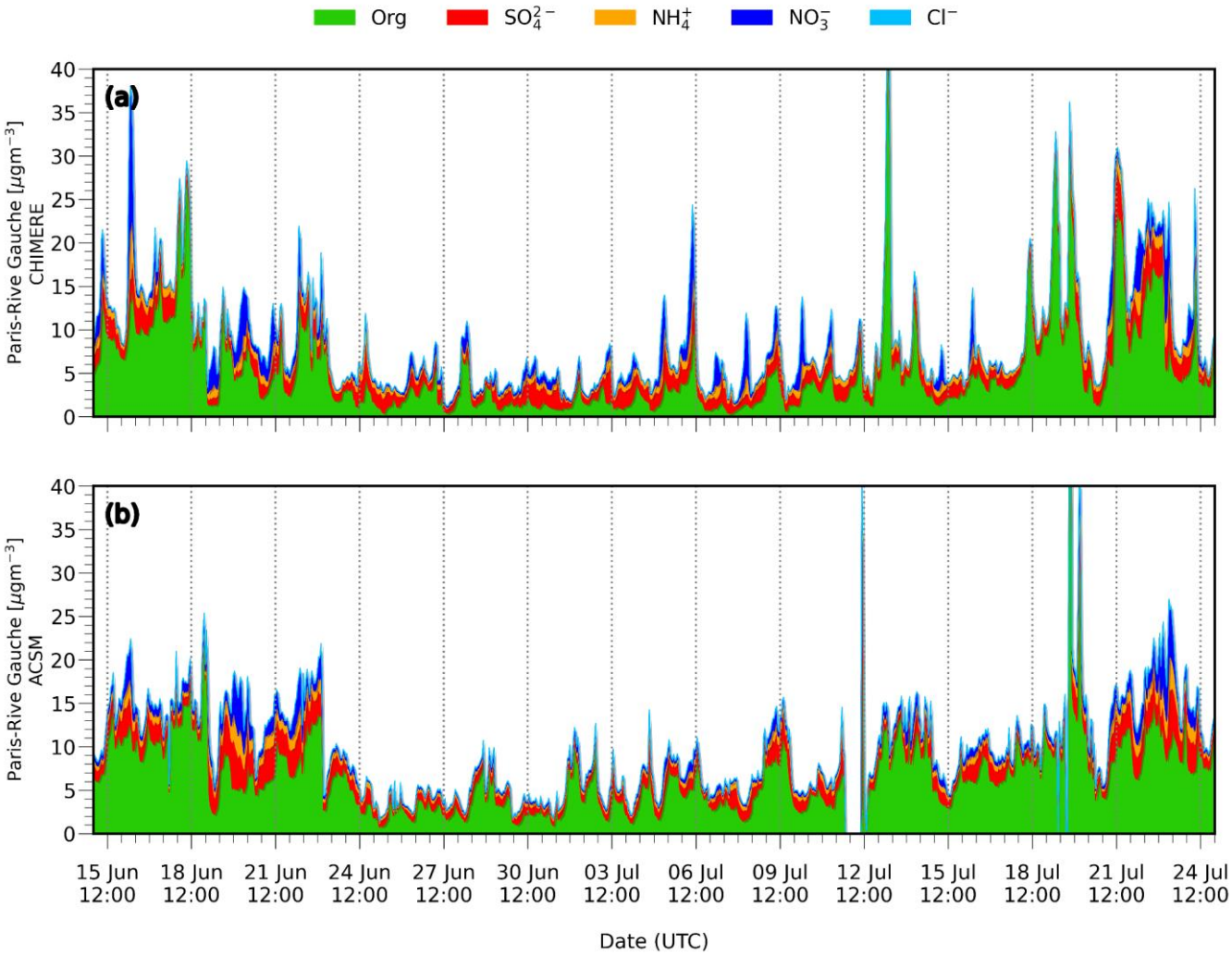

Figure S8: Time series of the chemical composition (organics, sulfate, nitrate, ammonium and chloride) simulated (a) and observed (b) at the Paris–Rive Gauche (PRG) urban background site.

,

:

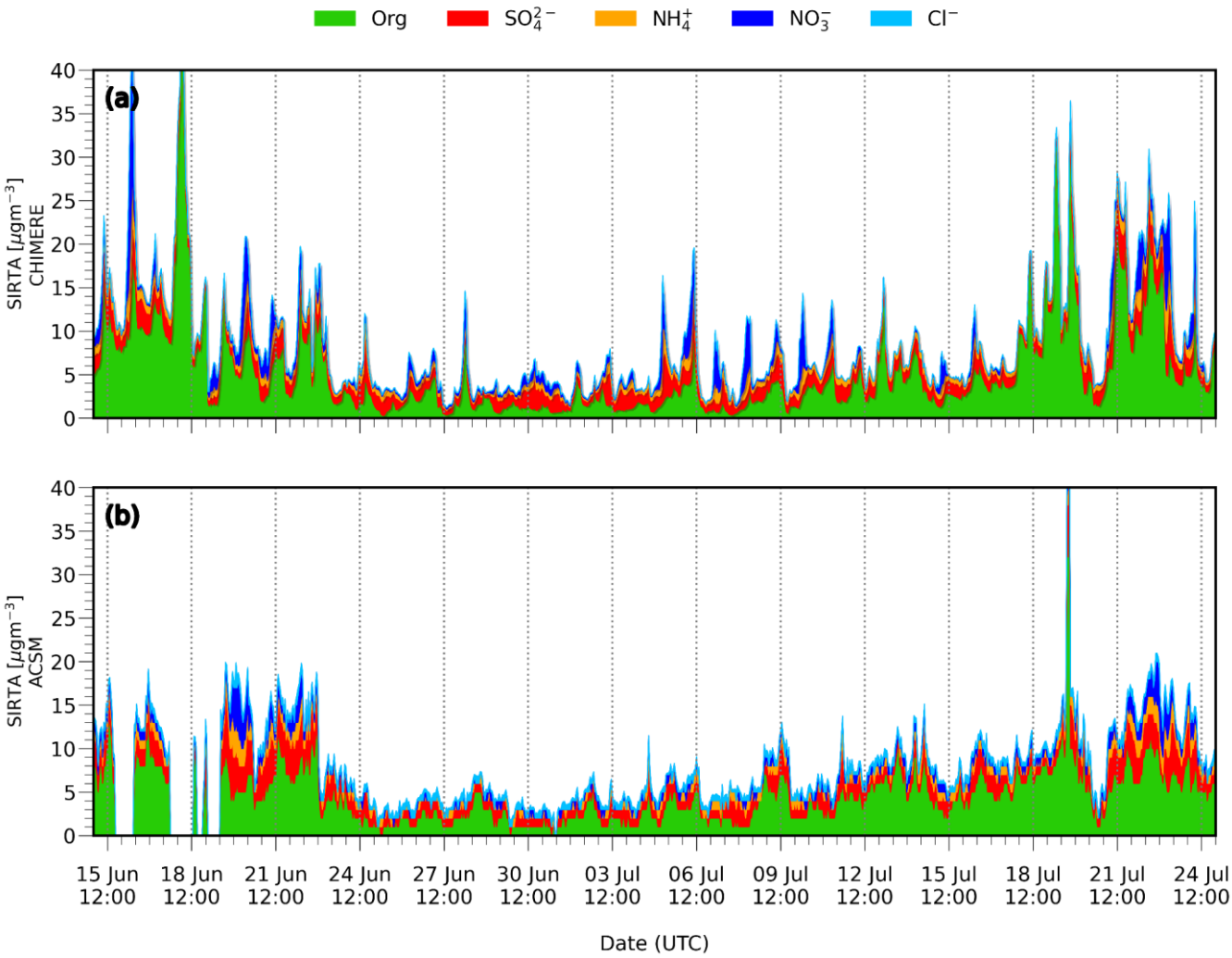

Figure S9: Time series of the chemical composition (organics, sulfate, nitrate, ammonium and chloride) simulated (a) and observed (b) at the SIRTA peri–urban site.

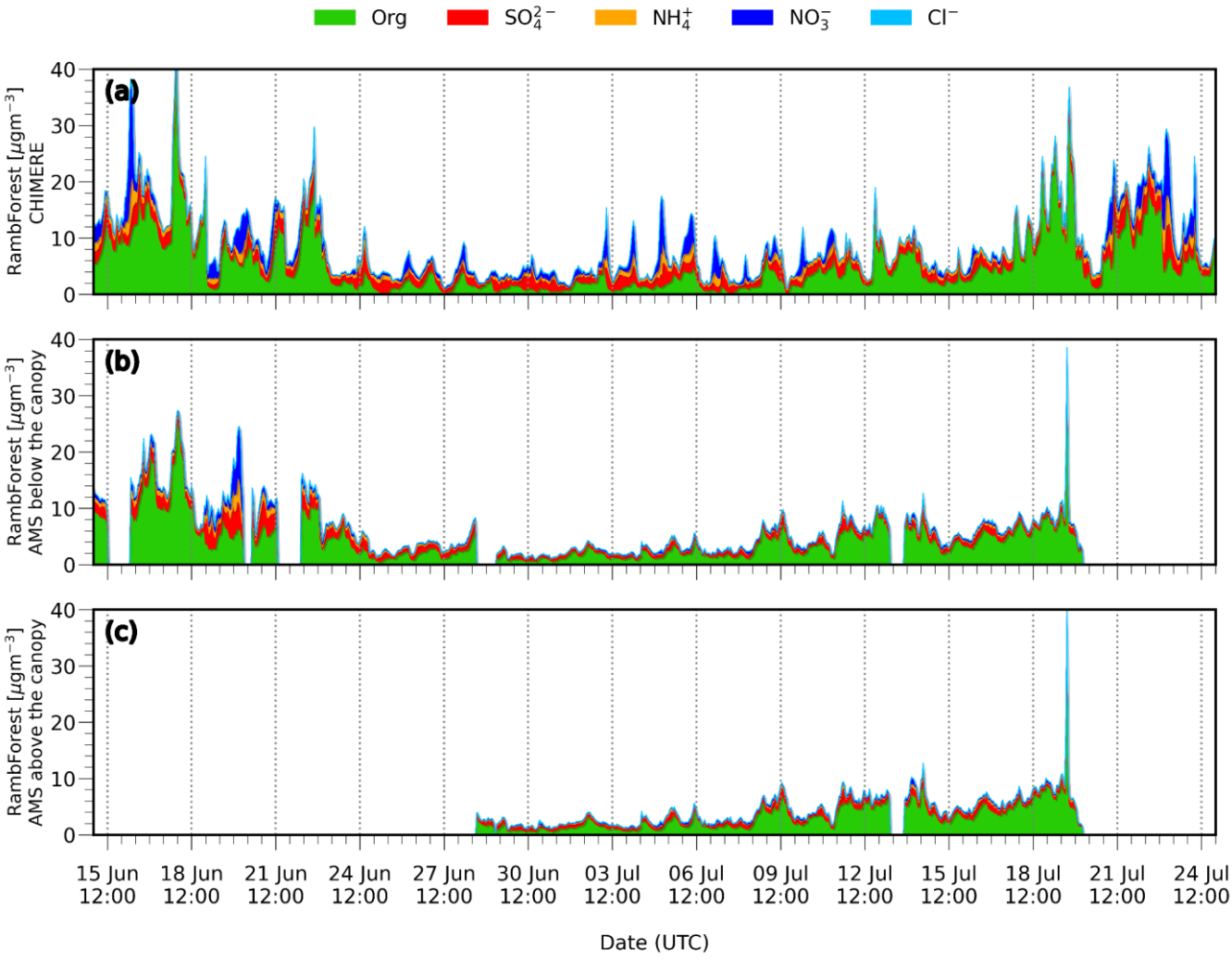

Figure S10: Time series of the chemical composition (organics, sulfate, nitrate, ammonium and chloride) simulated (a) and observed below the canopy (b) and above the canopy (c) at the Rambouillet forest (RambForest) site.

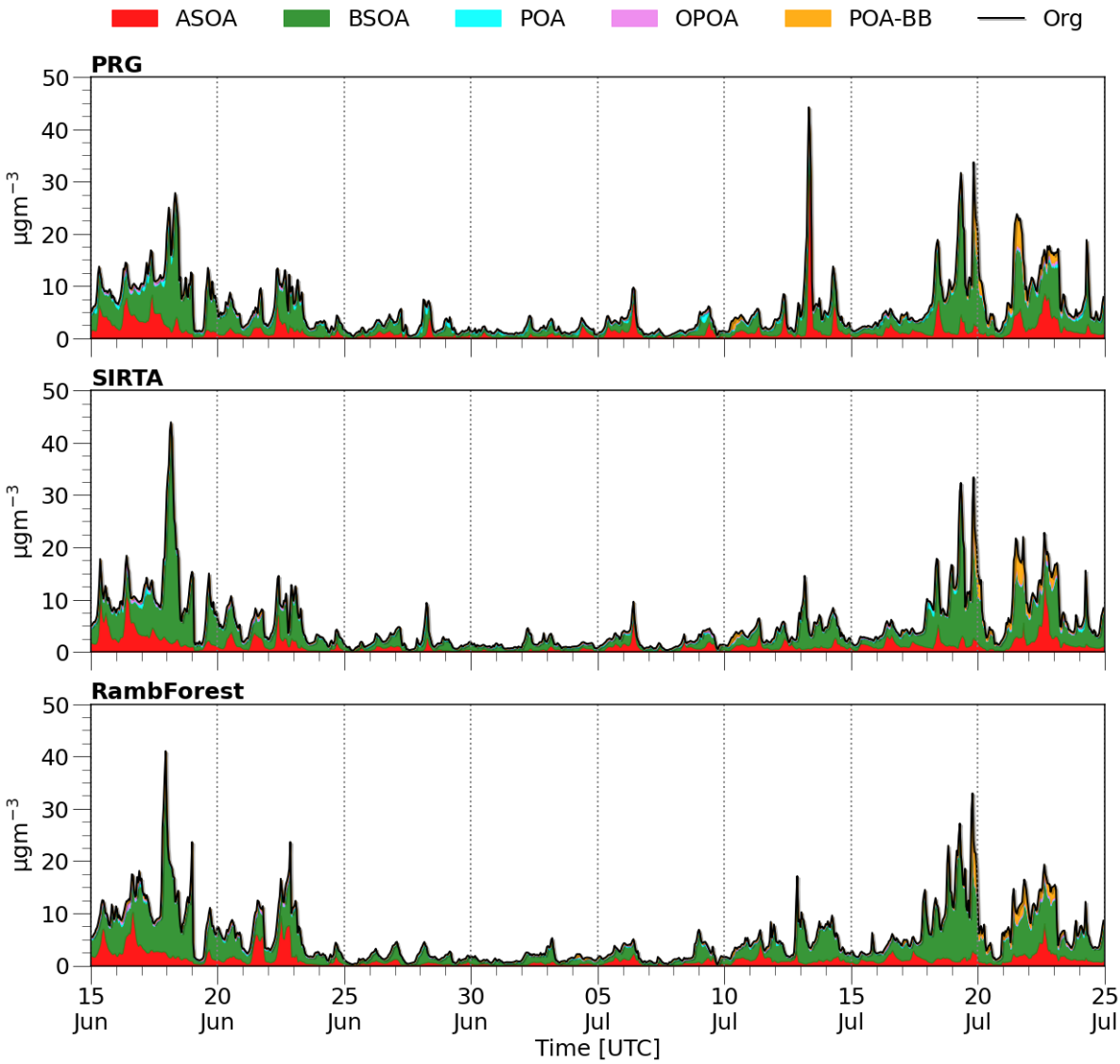

Figure S11: Simulated organic aerosol components during the ACROSS field campaign at the three different ACROSS sites. "ASOA" represents the anthropogenic organic aerosol, "BSOA" the biogenic organic aerosol, "POA" the primary organic aerosol, "OPOA" the oxidized POA (via OH), "POA-BB" the primary organic aerosol due to forest fires and "Org" the total organic aerosol.

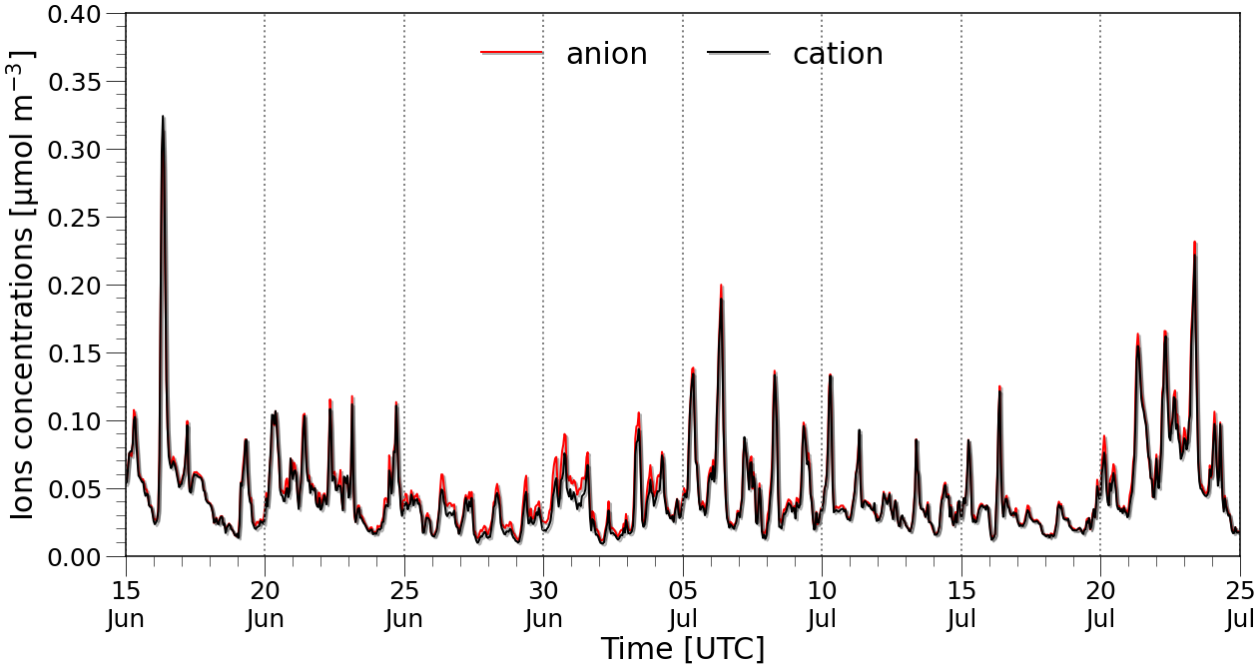

Figure S12: Time series of cation (Σ NH_4^+ + Na^+) and anion (Σ 2 SO_4^{2-} + NO_3^- + Cl^-) ions concentrations at the urban PRG site during the ACROSS period.

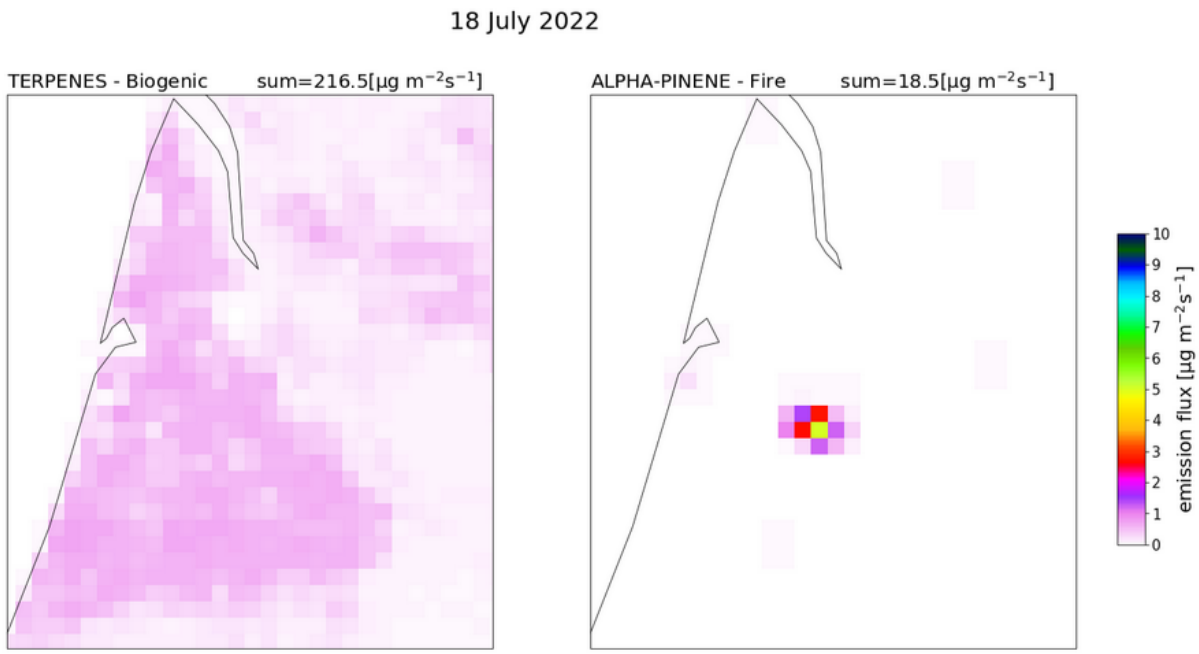

Figure S13: Daily-averaged emission fluxes of potential BSOA precursors: (left) terpenes (biogenic), and (right) α-pinene (fire) over the Gironde region (1.5°W-0.5°E, 43.8°N-45.5°N) for July 18, 2022. Fire emissions are vertically integrated.

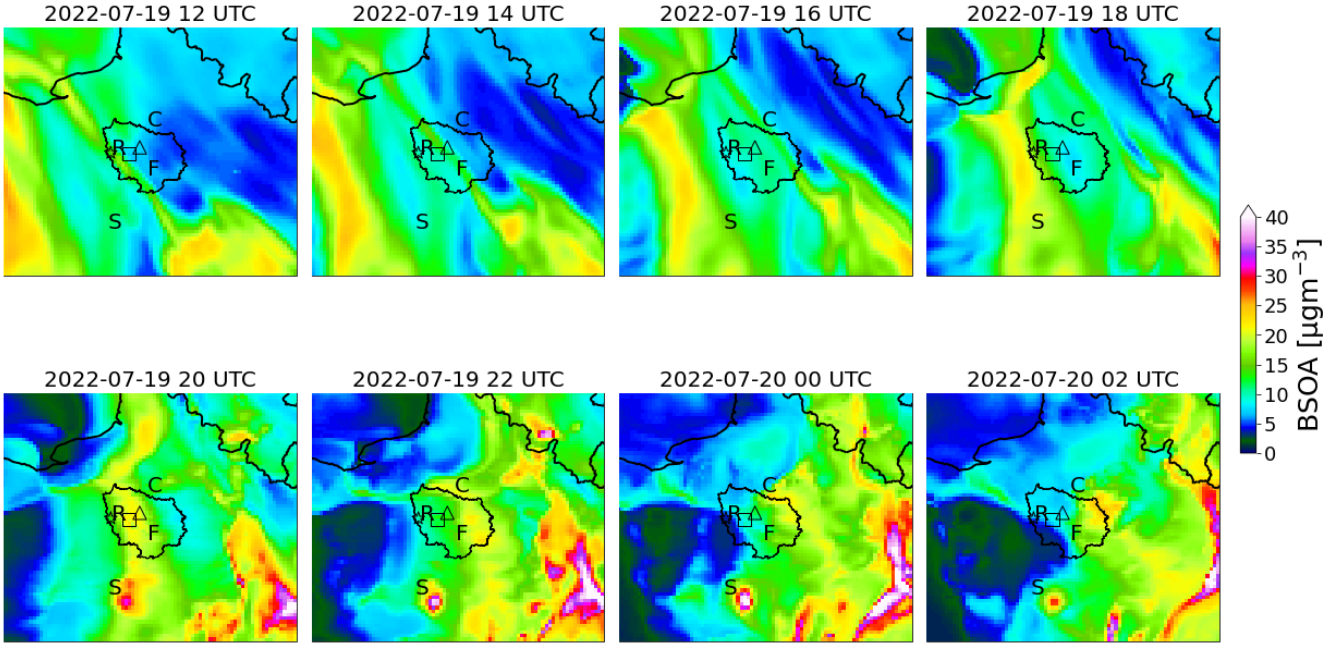

Figure S14: Simulated biogenic secondary organic aerosol (BSOA) mass concentrations for the 19 and 20 July 2022. "F" indicates the Fontainebleau forest, "R" the Rambouillet forest, "S" the Sologne forest and "C" the Chantilly forest. The star, the square and the triangle markers indicate respectively the RambForest, SIRTA and PRG sites. Please note that BSOA stems from BVOC compounds emitted by both fires and forests.

Name	Longitude (° E)	Latitude (° N)	Features
Calais	1.84	50.94	Urban
Creil	2.47	49.25	Urban
Metz	6.22	49.11	Urban
Paris Les Halles	2.34	48.86	Urban
Strasbourg	7.76	48.57	Urban
Poitiers	0.34	46.58	Urban
Lyon	4.85	45.75	Urban
Toulouse	1.43	43.62	Urban
Marseille	5.39	43.30	Urban

Table S1: GEOD'AIR sites available to validate the aerosol chemical composition.

	Full period (15 June– 25 July)				First heatwave (15 June–19 June)				Clean period (20 June–11 July)				Second heatwave (12 July–25 July)			
	N_{TOT}	R	MBE µg m^{-3}	NMB %	N_{TOT}	R	MBE µg m^{-3}	NMB %	N_{TOT}	R	MBE µg m^{-3}	NMB %	N_{TOT}	R	MBE µg m^{-3}	NMB %
Ammonium	943	0.52	0.06	8.2	120	0.39	0.11	12.8	524	0.40	0.10	16.5	299	0.71	–0.03	–3.9
Sulfate	942	0.25	–0.02	–1.2	120	–0.18	–0.21	–10.6	524	0.10	0.08	5.3	298	0.36	–0.11	–5.7
Nitrate	943	0.47	0.11	15.2	120	0.65	0.27	28.7	524	0.46	0.30	55.6	299	0.53	–0.29	–29.8
Organic	943	0.61	–1.39	–19.9	120	0.54	0.02	0.10	524	0.53	–1.78	–37.7	299	0.44	–1.26	–13.3
Chloride	943	0.14	–0.001	–1.7	120	0.56	–0.02	–45.2	524	–0.10	0.01	44.0	299	0.39	–0.02	–35.4
	OBS		MOD		OBS		MOD		OBS		MOD		OBS		MOD	
Ammonium	0.72		0.78		0.87		0.98		0.60		0.70		0.86		0.83	
Sulfate	1.66		1.64		2.9		1.79		1.42		1.50		1.93		1.82	
Nitrate	0.72		0.83		0.94		1.22		0.54		0.84		0.96		0.68	
Organic	6.97		5.58		10.60		10.61		4.71		2.93		9.46		8.20	
Chloride	0.04		0.04		0.04		0.02		0.03		0.05		0.06		0.04	

Table S2: Summary of the comparison of model output to observations for the PRG (urban) site from the ACSM; Statistical metrics are: NTOT, number of observations; R, correlation coefficient; MBE, mean bias error; NMB, normalized mean bias.

	Full period (15 June– 25 July)				First heatwave (15 June–19 June)				Clean period (20 June–11 July)				Second heatwave (12 July–25 July)			
	N_{TOT}	R	MBE µg m^{-3}	NMB %	N_{TOT}	R	MBE µg m^{-3}	NMB %	N_{TOT}	R	MBE µg m^{-3}	NMB %	N_{TOT}	R	MBE µg m^{-3}	NMB %
Ammonium	904	0.50	0.01	0.7	68	0.002	–0.15	–13.7	524	0.35	0.10	17.9	412	0.73	–0.13	–14.4
Sulfate	906	0.37	–0.22	–12.0	68	–0.37	–0.63	–22.9	526	0.20	–0.11	–6.9	312	0.64	–0.32	–15.6
Nitrate	906	0.39	0.13	21.0	68	0.13	–0.24	–28	526	037	0.33	63.8	312	0.50	–0.12	–15.5
Organic	906	0.68	–0.16	–3.1	68	0.08	1.93	22.6	526	0.65	–0.90	–24.5	312	0.52	0.64	9.1
Chloride	888	0.11	0.003	7.9	68	–0.01	–0.01	–38.1	511	–0.49	0.01	30.5	309	0.71	–0.01	–17.3
	OBS		MOD		OBS		MOD		OBS		MOD		OBS		MOD	
Ammonium	0.75		0.75		1.07		092		0.60		0.71		0.93		0.80	
Sulfate	1.86		1.63		2.73		2.10		1.62		1.51		2.07		1.74	
Nitrate	0.62		0.75		0.87		0.63		0.51		0.84		0.76		0.64	
Organic	5.18		5.03		8.54		10.48		3.68		2.78		7.00		7.64	
Chloride	0.038		0.041		0.035		0.021		0.037		0.048		0.041		0.033	

Table S3: As Table S2, but for the SIRTA (suburban) site

	Full period (15 June– 25 July)				First heatwave (15 June–19 June)				Clean period (20 June–11 July)				Second heatwave (12 July–25 July)			
	N_{TOT}	R	MBE µg m^{-3}	NMB %	N_{TOT}	R	MBE µg m^{-3}	NMB %	N_{TOT}	R	MBE µg m^{-3}	NMB %	N_{TOT}	R	MBE µg m^{-3}	NMB %
Above the canopy																
Ammonium	506	0.07	0.46	251.8	–				319	0.16	0.57	396.0	187	0.36	0.26	106.5
Sulfate	506	0.01	0.67	95.9	–				319	0.01	0.81	130.7	187	0.31	0.43	51.3
Nitrate	506	0.21	0.52	325.4	–				319	0.52	0.84	632.7	187	0.17	–0.02	–6.9
Organic	506	0.62	0.7	21.3	–				319	0.57	–0.04	–1.7	187	0.41	1.99	36.7
Chloride	506	0.139	0.015	59.4	–				319	0.12	0.027	99.6	187	0.20	–0.005	–21.4
Below the canopy																
Ammonium	772	0.27	0.33	89.3	101	0.18	0.19	23.3	484	0.22	0.40	123.2	187	0.43	0.24	93.0
Sulfate	772	0.17	0.40	36.7	101	–0.12	–0.18	–8.8	484	0.11	0.51	51.4	187	0.38	0.44	53.3
Nitrate	772	0.29	0.48	148.1	101	0.25	0.64	105.5	484	0.32	0.64	214.4	187	0.45	–0.035	–15.3
Organic	772	0.77	0.45	9.7	101	0.76	1.22	11.9	484	0.76	–0.13	–4.5	187	0.43	1.52	26.0
Chloride	772	0.06	0.01	32.8	101	0.61	–0.021	67.6	484	–0.08	0.02	67.6	187	0.39	0.0	–1.4

	OBS	MOD	OBS	MOD	OBS	MOD	OBS	MOD
Ammonium	0.18/0.38	0.64/0.71	0.83	1.02	0.14/0.33	0.71/0.73	0.25/0.26	0.51/0.61
Sulfate	0.70/1.09	1.38/1.49	2.08	1.90	0.63/0.99	1.45/1.49	0.83/0.82	1.26/1.26

Nitrate	0.16/0.32	0.69/0.80	0.61	1.25	0.13/0.30	0.97/0.94	0.21/0.23	0.19/0.19
Organic	3.34/4.59	4.05/5.04	10.35	11.58	2.13/2.90	2.09/2.77	5.40/5.87	7.39/7.40
Chloride	0.025/0.031	0.040/0.041	0.052	0.028	0.027/0.031	0.05/0.053	0.023/0.018	0.018/0.017

Table S4: As Table S2, but for the RambForest site using using AMS measurements. Average concentrations are reported for both above and below the canopy, respectively, divided by a slash sign.

	Full period (15 June– 25 July)				First heatwave (15 June–19 June)				Clean period (20 June–11 July)				Second heatwave (12 July–25 July)			
	N_{TOT}	R	MBE µg m^{-3}	NMB %	N_{TOT}	R	MBE µg m^{-3}	NMB %	N_{TOT}	R	MBE µg m^{-3}	NMB %	N_{TOT}	R	MBE µg m^{-3}	NMB %
eBC	70	0.50	0.11	25	10	0.60	0.20	34	36	0.17	0.12	40	23	0.53	–0.001	–0.1
EC	70	0.41	0.11	25	10	0.62	0.18	29	36	–0.04	0.14	48	23	0.36	–0.002	–3.5
OM	71	0.73	–0.17	–3	10	0.53	2.2	27	37	0.50	–1.2	–31	23	0.58	0.5	7
	OBS		MOD		OBS		MOD		OBS		MOD		OBS		MOD	
eBC	0.45		0.56		0.60		0.80		0.31		0.43		0.59		0.59	
EC	0.45				0.62				0.29				0.61			
OM	5.8		5.6		8.2		10.3		4.0		2.76		7.6		8.1	

Table S5: Summary of the comparison of the black carbon concentrations for the PRG (urban) site averaged on the filter sampling times (daytime 6 – 20 UTC, night time 20 – 6 UTC). eBC has been corrected for the ACTRIS harmonisation factor (H*=2.45). OC has been converted to OM assuming an OM/OC ratio equal to 1.8. Statistical metrics are: NTOT number of observations, R correlation coefficient, MBE mean bias error, NMB normalized mean bias.

	Full period (15 June– 25 July)				First heatwave (15 June–19 June)				Clean period (20 June–11 July)				Second heatwave (12 July–25 July)			
	N_{TOT}	R	MBE µg m^{-3}	NMB %	N_{TOT}	R	MBE µg m^{-3}	NMB %	N_{TOT}	R	MBE µg m^{-3}	NMB %	N_{TOT}	R	MBE µg m^{-3}	NMB %
eBC	36	0.28	0.1	64	–				17	0.36	0.13	130	19	0.13	0.07	36
EC	38	0.38	0.1	60	–				17	0.3	0.13	130	21	0.32	0.07	34
rBC	21	0.45	0.17	153	–				1	–	–	–	20	0.47	0.16	147
OM	40	0.82	0.18	4	–				19	0.70	–1.10	–29	21	0.70	1.27	19
	OBS		MOD		OBS		MOD		OBS		MOD		OBS		MOD	
eBC	0.15		0.25		–				0.10		0.22		0.20		0.27	
EC	0.16				–				0.10				0.21			
rBC	0.11				–				0.08				0.11			
OM	5.17		5.36		–				3.42		2.42		6.74		8.01	

Table S6: As for Table S5, but for the RambForest (forest) site.

References

Carter, W. P. L.: Development of the SAPRC-07 chemical mechanism, Atmos. Environ., 44, 5324–5335, https://doi.org/10.1016/j.atmosenv.2010.01.026, 2010.

Cholakian, A., Beekmann, M., Colette, A., Coll, I., Siour, G., Sciare, J., Marchand, N., Couvidat, F., Pey, J., Gros, V., Sauvage, S., Michoud, V., Sellegri, K., Colomb, A., Sartelet, K., Langley DeWitt, H., Elser, M., Prévot, A. S. H., Szidat, S., and Dulac, F.: Simulation of fine organic aerosols in the western Mediterranean area during the ChArMEx 2013 summer campaign, Atmospheric Chem. Phys., 18, 7287–7312, https://doi.org/10.5194/acp-18-7287-2018, 2018.

Di Antonio, L. and Siour, G.: ACROSS_LISA_WRF-CHIMERE_HYSPLIT_Backtraj_1H, https://doi.org/10.25326/543, 2023.

Murphy, B. N. and Pandis, S. N.: Simulating the Formation of Semivolatile Primary and Secondary Organic Aerosol in a Regional Chemical Transport Model, Environ. Sci. Technol., 43, 4722–4728, https://doi.org/10.1021/es803168a, 2009.

Shrivastava, M., Zelenyuk, A., Imre, D., Easter, R., Beranek, J., Zaveri, R. A., and Fast, J.: Implications of low volatility SOA and gas-phase fragmentation reactions on SOA loadings and their spatial and temporal evolution in the atmosphere, J. Geophys. Res. Atmospheres, 118, 3328–3342, https://doi.org/10.1002/jgrd.50160, 2013.

Shrivastava, M., Easter, R. C., Liu, X., Zelenyuk, A., Singh, B., Zhang, K., Ma, P.-L., Chand, D., Ghan, S., Jimenez, J. L., Zhang, Q., Fast, J., Rasch, P. J., and Tiitta, P.: Global transformation and fate of SOA: Implications of low-volatility SOA and gas-phase fragmentation reactions, J. Geophys. Res. Atmospheres, 120, 4169–4195, https://doi.org/10.1002/2014JD022563, 2015.

Zhang, Q. J., Beekmann, M., Drewnick, F., Freutel, F., Schneider, J., Crippa, M., Prevot, A. S. H., Baltensperger, U., Poulain, L., Wiedensohler, A., Sciare, J., Gros, V., Borbon, A., Colomb, A., Michoud, V., Doussin, J.-F., Denier van der Gon, H. a. C., Haeffelin, M., Dupont, J.-C., Siour, G., Petetin, H., Bessagnet, B., Pandis, S. N., Hodzic, A., Sanchez, O., Honoré, C., and Perrussel, O.: Formation of organic aerosol in the Paris region during the MEGAPOLI summer campaign: evaluation of the volatility-basis-set approach within the CHIMERE model, Atmospheric Chem. Phys., 13, 5767–5790, https://doi.org/10.5194/acp-13-5767-2013, 2013.